SIMULATION OF PELLET-CLADDING THERMOMECHANICAL INTERACTION AND FISSION GAS RELEASE

A. DENIS, A. SOBA
Departamento Combustibles Nucleares,
Comisión Nacional de Energía Atómica,
Buenos Aires, Argentina

Abstract

This paper summarizes the present status of a computer code that describes some of the main phenomena occurring in a nuclear fuel element throughout its life. Temperature distribution, thermal expansion, elastic and plastic strains, creep, mechanical interaction between pellet and cladding, fission gas release, swelling and densification are modelized. The code assumes an axi-symmetric rod and hence, cylindrical finite elements are employed for the discretization. Due to the temperature dependence of the thermal conductivity, the heat conduction problem is non-linear. Thermal expansion gives origin to elastic or plastic strains, which adequately describe the bamboo effect. Plasticity renders the stress–strain problem non linear. The fission gas inventory is calculated by means of a diffusion model, which assumes spherical grains and uses a finite element scheme. In order to reduce the calculation time, the rod is divided into five cylindrical rings where the temperature is averaged. In each ring the gas diffusion problem is solved in one grain and the results are then extended to the whole ring. The pressure, increased by the released gas, interacts with the stress field. Densification and swelling due to solid and gaseous fission products are also considered. Experiments, particularly those of the FUMEX series, are simulated with this code. A good agreement is obtained for the fuel center line temperature, the inside rod pressure and the fractional gas release.

1. INTRODUCTION

Among the numerous phenomena that take place during operation of a fuel element, thermomecanical interaction between pellet and cladding and fission gas release have historically deserved special attention. These phenomena are interconnected and mutually dependent. On the one hand, due to the low thermal conductivity of the fuel material, a quite steep temperature gradient appears in the pellet. The high temperatures developed within the pellet, especially at its center, give rise to thermal expansion. The strain produced in the pellet may be either of the elastic or plastic types. For sufficiently long periods, creep may also have a significant effect. As a consequence, the initially cylindrical pellet surface distorts, bending outwards, the top and bottom faces being displaced further than the central belt [1]. The dimensional changes in the fuel rod provoked by thermal expansion may induce pellet-cladding interaction (PCI) and the consequent plastic cladding strain [2]. To simulate this problem the thermal–elastic–plastic coupled equations have to be solved. On the other hand, fission products accumulate within the pellet. Among them, the gaseous products, namely Xe and Kr, represent about 30%. Their almost complete insolubility in the UO_2 matrix is responsible for the formation of bubbles, either intra and intergranular. They decrease the thermal conductivity of the fuel, and consequently its temperature increases. An important fraction of the gas generated accumulates in the intergranular bubbles, until they saturate and release the gas in excess to the plenum and the gap. In this manner, it contributes to increase the internal pressure in the fuel element, modifies the gap thickness and affects the thermal conductance of the gap.

The code presented here solves first the heat diffusion equation and gives the temperature distribution in the pellet, the gap and the cladding. To this end, a finite element scheme in

cylindrical coordinates is used. Its solution is the input to the stress-strain problem. For simplicity, the system is divided into five cylindrical rings, according to the temperature range. In each ring the gas diffusion problem is solved in an ideal, spherical grain.

2. THE MODELIZATION

2.1 The thermal problem

Since the system is assumed to have axial symmetry, cylindrical coordinates are employed. The temperature depends on r and z only. If T represents the temperature, Q is the volumetric heat generation rate, $\kappa = \kappa(T)$ is the thermal conductivity and assuming steady-state heat transfer conditions, the temperature distribution in each material is obtained by solving the differential equation:

$$\kappa\left(\frac{1}{r}\frac{\partial}{\partial r}(r\frac{\partial T}{\partial r})+\frac{\partial^2 T}{\partial z}\right)+Q=0$$

with the boundary conditions: T = constant at the cladding external radius (Dirichlet condition) and $\nabla T = 0$ (Neumann condition) at the remaining portion of the system boundary. These together with the power history, represent the input data.

Application of the finite element method involves definition of a mesh, which in this case is chosen of triangular elements, definition of the corresponding shape functions and approximation of the continuous unknown function T by a linear combination of the shape functions. A system of linear equations is finally obtained one equation for each unknown nodal value.

For the thermal conductivity of UO_2 the following expression was used [1]:

$$\kappa(T)=\frac{1}{0.034944+2.2430\times10^{-4}T}+\frac{6.157\times10^{9}}{T^2}\exp\left[-\frac{1.41\times1.6\times10^{-19}}{kT}\right]$$

with T in K and κ in $W\,m^{-1}K^{-1}$. The temperature dependence of κ is responsible for the non–linearity of the thermal problem and hence the temperature is calculated by an iterative procedure. The solution of the heat transfer problem becomes the input to the stress analysis. The same discretization is used to solve both.

2.2. The stress-strain analysis

2.2.1. Elasticity and plasticity

The Hill's theory of plasticity together with the flux rules of Levy Prandtl-von Mises provide the following relation for the plastic strain [3]

$$\Delta\varepsilon^p_{rr}=\frac{\Delta\varepsilon_p}{2\sigma_e}(2\sigma_{rr}-\sigma_{zz}) \quad ; \quad \Delta\varepsilon^p_{zz}=\frac{\Delta\varepsilon_p}{2\sigma_e}(2\sigma_{zz}-\sigma_{rr}) \quad ; \quad \Delta\varepsilon^p_{rz}=\frac{3\Delta\varepsilon_p}{2\sigma_e}\sigma_{rz}$$

The equivalent stress,

$$\sigma_e = (\sigma_{rr}^2 + \sigma_{zz}^2 - \sigma_{rr}\sigma_{zz} + 3\sigma_{rz}^2)^{1/2}$$

and the equivalent strain, $\Delta\varepsilon_p$, are related by an experimental curve characteristic of each material, where the segment corresponding to small stresses and strains is linear and represents the elastic range. For large strains this relation is non-linear and hence an iterative procedure is necessary for the calculations.

2.2.2. Creep

The creep analysis is carried out by means of the flux rules of Levy Prandtl-von Mises and the Norton law [4]

$$\dot{\varepsilon} = K\sigma^m$$

where K and m depend on the material. The values $K = 10^{-6}\text{MPa}^{-3}\text{d}^{-1}$ and m=3 [5] were used in the present work.

2.2.3. The constitutive equations

Given the axial symmetry of the system, neither the geometry nor the surface loading depend on the angular coordinate. The displacements, strains and stresses are functions of r and z only. Let us represent with u and w the displacements in the r and z direction, respectively. The strain-displacement relations are [6]:

$$e_{rr} = \frac{\partial u}{\partial r}\ ;\ e_{\theta\theta} = \frac{u}{r}\ ;\ e_{zz} = \frac{\partial w}{\partial z}\ ;\ e_{rz} = \frac{\partial u}{\partial z} + \frac{\partial w}{\partial r}\ ;\ e_{r\theta} = 0\ ;\ e_{z\theta} = 0$$

The column vector $\{e\}$ contains the four non-zero components of the strain:

$$\{e\}^T = [e_{rr} \quad e_{\theta\theta} \quad e_{zz} \quad e_{rz}]$$

It has four contributions: thermal $\{\varepsilon_{th}\}$, elastic $\{\varepsilon\}$, plastic $\{\varepsilon_p\}$ and creep $\{\varepsilon_c\}$

$$\{e\} = \{\varepsilon_{th}\} + \{\varepsilon\} + \{\varepsilon_p\} + \{\varepsilon_c\}$$

where the first two are expressed as:

$$\{\varepsilon_{th}\}^T = [\alpha\Delta T \quad \alpha\Delta T \quad \alpha\Delta T \quad 0] \text{ and } \{\varepsilon\}^T = [\varepsilon_{rr} \quad \varepsilon_{\theta\theta} \quad \varepsilon_{zz} \quad \varepsilon_{rz}]$$

and α is the thermal expansion constant. The components of the elastic strain are related with the stress by the Hooke law

$$\{\sigma\} = [D]\{\varepsilon\}$$

where the components of the stress vector are:

$$\{\sigma\}^T = [\sigma_{rr} \quad \sigma_{\theta\theta} \quad \sigma_{zz} \quad \sigma_{rz}]$$

and $[D]$ is the material matrix, which components are determined with the Young's modulus and the Poisson's ratio.

The plastic term is obtained by a recursive procedure in which the values of stress and strain are fitted to the uniaxial curve corresponding to the material involved. In the case of the present study, in the temperature range involved, only the Zry exhibits a significant plastic deformation.

When the finite element method is applied, the unknown displacements u and w are written in terms of the element nodal values and the shape functions. The above differential equations are thus transformed to linear equations, which are formally similar to those for the thermal problem.

The physical constants employed in the present calculations [7] are listed in Table I.

TABLE I. ELASTIC AND THERMAL CONSTANTS USED IN THE CODE

Young's modulus E (Pa)	UO_2: $2.065\text{x}10^{11}$ $(1+1.091\text{x}10^{-4}\ T)$ Zry: $1.236\text{x}10^{11} - 6.221\text{x}10^{7}\ T$
Poisson's ratio μ	UO_2: 0.316 Zry: 0.32
Thermal expansion α (K^{-1})	UO_2: $(-4.972\text{x}10^{-4} + 7.107\text{x}10^{-6}\ T + 2.583\text{x}10^{-9}\ T^2)/\Delta T$ Zry: $(-2.07\text{x}10^{-3} + 6.72\text{x}10^{-6}\ T)/\Delta T$
Thermal conductivity κ ($W\ m^{-1}K^{-1}$)	UO_2: $\left[\frac{4.04\times10^{3}}{464+T} + 1.216\text{x}10^{-2}\exp(1.867\text{x}10^{-3}T)\right]$ Zry: $7.51 + 2.09\text{x}10^{-2}\ T - 1.45\text{x}10^{-5}\ T^2 + 7.67\text{x}10^{-9}\ T^{-3}$ He: $0.3366\ T^{0.668}$

Temperatures T in K.

2.3 The fission gas release problem

The fission gas model, which was already outlined in some previous works [7, 8], is based on the following hypotheses:

- ☆ The UO_2 fuel is considered as a collection of spherical grains where, due to continuous irradiation, noble gas atoms are produced by fission of the U atoms.
- ☆ Due to the virtually complete insolubility of these gases in the UO_2 matrix, they either precipitate within the grains forming bubbles of a few nanometers (intragranular bubbles) or are released to the grain boundaries forming intergranular, lenticular bubbles, with sizes of some microns.
- ☆ Diffusion is the rate-controlling step.
- ☆ Intragranular bubbles are considered immobile and acting as traps for the diffusing gas.
- ☆ Irradiation can cause destruction of both types of bubbles.

- ☆ The gas atoms contained in the destroyed intragranular bubbles return to the diffusion process. Due to kinetic reasons, a dynamical solubility, much higher than that predicted by the equilibrium diagram is established.
- ☆ Destruction of intergranular bubbles acts as an additional source of gas atoms that affect mainly the region of the grain adjacent to the grain boundary.
- ☆ The amount of gas stored in the grain boundary bubbles grows up to a saturation value. Then, these bubbles interconnect and the gas in excess is released to the plenum and to the gap between fuel and cladding.
- ☆ The grains grow due to the high temperature of the fuel, especially near its center. The grain boundary traps the gas, either free or in bubbles, in the swept volume.

The rate of gas release is calculated by means of the diffusion equation in spherical coordinates, with sources and traps:

$$\frac{\partial c}{\partial t} = D\left(\frac{\partial^2 c}{\partial r^2} + \frac{2}{r}\frac{\partial c}{\partial r}\right) - gc + bm + \beta$$

together with the balance equation for trapped atoms:

$$\frac{\partial m}{\partial t} = gc - bm$$

where c and m are the concentrations of free and trapped gas atoms (at/m^3), ß is the gas generation rate (at/m^{3}s), g and b are the probabilities of capture and release by traps (at/s) and D is the diffusion coefficient of the single gas atoms in the UO_2 matrix. Assuming stationary trapping conditions: $gc-bm=0$ and defining the total gas concentration of gas in the grain $\psi=c+m$ and the effective diffusion coefficient $D'=Db/(b+g)$, the equivalent equation

$$\frac{\partial \psi}{\partial t} = D'\left(\frac{\partial^2 \psi}{\partial r^2} + \frac{2}{r}\frac{\partial \psi}{\partial r}\right) + \beta$$

is obtained, with the boundary conditions: $\psi(r=a)=0$, i.e., the grain boundary at $r=a$ acts as a perfect sink, and $\partial\psi/\partial r=0$ at $r=0$ due to spherical symmetry.

The diffusion coefficient D was given by Turnbull et al.[9]; the bubbles' size and concentration, and the trapping parameters, g and b, are due to White et al. [10]; the equiaxed grain growth rate is that used by Ito et al.[2].

The saturation concentration of the grain boundary, N_S, is calculated assuming that the gas in the intergranular bubbles obeys the ideal gas law, that the gas pressure, the external stress and the surface tension are in equilibrium and that bubbles interconnection occurs when a given fraction, f_S, of the grain boundary area is covered. The value $f_S=0.5$ is usually assigned. However, it seems appropriate to assume that bubbles interconncetion occurs as a percolation process. To this end, let us consider the grain boundary area divided into regular triangles and let us put circles, of radius equal to half the triangle side, in some of the crossing lines that form the triangles. The elementary theory predicts that the percolation threshold occurs when half of the sites are occupied [14]. This corresponds to a fraction of covered area $f_S = \pi\sqrt{3}/12 = 0.453$.

The function representing the gas production rate, $\beta(r)$, was already given in. It contains the uniform gas generation rate due to irradiation, obtained from the fission rate, F (fissions/m^{3}s), times the gas production yield, y, and the contribution due to resolution of intergranular bubbles, which is proportional to the occupation of the grain boundary, N. Its expression is:

$$\beta = \begin{cases} yF & \text{for } 0 \le r \le a-2\lambda \\ yF+h(r) & \text{for } a-2\lambda < r \le a \end{cases}$$

where λ represents the penetration depth of the redissolved atoms and the function $h(r)$ is such that

$$\int_{a-2\lambda}^{a} h(r) 4\pi r^2 dr = 4\pi a^2 b' \frac{N}{2}$$

where N indicates the number of gas atoms per unit area of the grain boundary.

An appropriate choice for $h(r)$ is a Gauss function. For simplicity, a triangular approximation was used [16]. The proportionality constant b'(1/s) represents the probability of resolution of the intergranular bubbles and is one of the parameters of the model.

Before saturation, the gas content per unit area of the grain boundary, N_k, at the time t_k is obtained from a balance equation that includes the gas contained in the grain volume at t_{k-1}

$$C_{k-1} = 4\pi \int_0^{a_{k-1}} r^2 \psi_{k-1} dr ,$$

the gas contained in the grain boundary at t_{k-1}

$$4\pi a_{k-1}^2 \frac{N_{k-1}}{2} ,$$

the amount of gas generated by fission during Δt_k

$$\frac{4}{3}\pi a_k^3 \, y \, F_k \, \Delta t_k ,$$

the amount of gas incorporated to the grain and grain boundary by sweeping of the grain boundary

$$\left(C_{k-1} + 4\pi a_{k-1}^2 \frac{N_{k-1}}{2} \right) \left(\frac{a_k^3 - a_{k-1}^3}{a_{k-1}^3} \right)$$

and the gas contained in the grain volume at t_k (C_k). The balance equation is

$$\left(C_{k-1} + 4\pi a_{k-1}^2 \frac{N_{k-1}}{2} \right) \left(\frac{a_k^3}{a_{k-1}^3} \right) + \frac{4}{3}\pi a_k^3 \, y \, F_k \, \Delta t_k = C_k + 4\pi a_k^2 \frac{N_k}{2}$$

which, with the initial conditions (t=0, k=0) C_0=0 and N_0=0 yields N_k at every instant t_k. Before saturation N_k represents the gas content of the grain boundary. After saturation the grain boundary content is set equal to N_S and the difference $N_k - N_S$ times the grain boundary area gives the number of gas atoms released to the free volume. This number is determined by

$$R_k = max\left(\frac{4\pi a_k^2}{2}(N_k - N_S), R_{k-1}\right)$$

which prevents the decrease of R_k when the temperature decreases.

2.4. Swelling

The contribution to swelling of intragranular and intergranular gas bubbles and of fission products dissolved in the lattice is considered. In the first case, if a concentration C_B of intragranular bubbles is created and if they are assumed to have the same radius R_B, the swelling they produce is

$$\left.\frac{\Delta V}{V}\right|_{\text{int.bub.}} = \frac{(4/3)\pi R_B^3 C_B}{1-(4/3)\pi R_B^3 C_B} \approx (4/3)\pi R_B^3 C_B$$

The concentration C_B is initially zero and grows up to an stationary value, provided that the irradiation conditions are kept constant. This implies that the swelling due to this type of bubbles reaches a saturation value.

To determine the swelling due to intergranular bubbles, we assume that the gas in a bubble obeys the ideal gas law and that the gas pressure balances the external pressure, P_{ext}, and the stress due to surface tension $2\gamma/r_f$, where r_f indicates the radius of curvature of the bubble's faces. The swelling produced when a surface concentration N of gas atoms is established in the boundary of a grain of radius a is

$$\left.\frac{\Delta V}{V}\right|_{\text{g.b.bub}} = \frac{3kTN}{2a(2\gamma/r_f + P_{ext})}$$

Given that the concentraion N reaches a saturation value, the swelling due to intergranular bubbles also saturates. On the contrary, the volume increase due to fission products, either solid or gaseous, dissolved in the lattice, either in interstitial or substitutional sites, although smaller than that due to gas bubbles, maintains a steady growth. As a rough estimate, we assume that the swelling due to fission products in the lattice is described by the empirical relation

$$\left.\frac{\Delta V}{V}\right|_{\text{l.f.p.}} = 0.0032\,\text{Bup[at\%]}$$

2.5. Densification

In the simple densification model used in the present work the porous solid is represented by an assembly of spherical grains which contain a density of spherical pores of equal radius

uniformly distributed in the solid. The pores are assumed to be small compared to the grain size and small compared to the interpore spacing. The fission fragments, passing near a pore, provoke the emission of vacancies to the lattice, which then diffuse to the grain boundary. This process is similar to the resolution of gas bubbles but given that the pores size is considerably larger than that of the bubbles, it is unlikely that a pore can be completely converted to vacancies by a single resolution event. Resolution is rather considered to reduce the size of the pores. However, due to the similarity of both processes we can assume that the probability that a vacancy in a pore will be ejected into the lattice takes a value similar to the rate of bubbles resolution, *b*. With all these assumptions we obtain the time dependence of porosity [17]

$$P = P_0 e^{-bt}$$

where P_0 represents the initial porosity. From here, the fractional volume change due to densification results

$$\left.\frac{\Delta V}{V}\right|_{\text{dens.}} = -\frac{P_0(1-e^{-bt})}{1-P_0 e^{-bt}} \approx -P_0(1-e^{-bt})$$

which is similar to the expression used in Refs. [18].

The total fractional volume change due to swelling and densification is obtained as the sum of these four contributions. This gives origin to an extra strain term

$$\varepsilon_{s.d.} = \frac{1}{3}\left[\left.\frac{\Delta V}{V}\right|_{\text{int.bub.}} + \left.\frac{\Delta V}{V}\right|_{\text{g.b.bub.}} + \left.\frac{\Delta V}{V}\right|_{\text{l.f.p.}} + \left.\frac{\Delta V}{V}\right|_{\text{dens.}}\right]$$

which is added to the thermal, elastic, plastic and creep contributions.

3. RESULTS AND DISCUSSION

With the code just described the six FUMEX experiments were simulated. The real power histories were conveniently simplified to save calculation time. Figures 1-6 show the input data and the results obtained with the code for the central line temperature, the internal rod pressure and the fractional release. The comparison between some results of our calculations and the coresponding data presented in the final report of the FUMEX experiment [19] are summarized in Table II.

The values shown in Table II reveal that the results obtained with our code fit quite well to the experimental results and in all the cases, except the final ramp of experiment 6S, fall within the range of values obtained with the other codes. As it was expected, the fitting is better in the cases of constant or nearly constant power.

The calculation time required to simulate these experiments, with power histories simplified to about 50 power steps, was about 10 minutes in a personal computer with a 330 MHz, Pentium II processor.

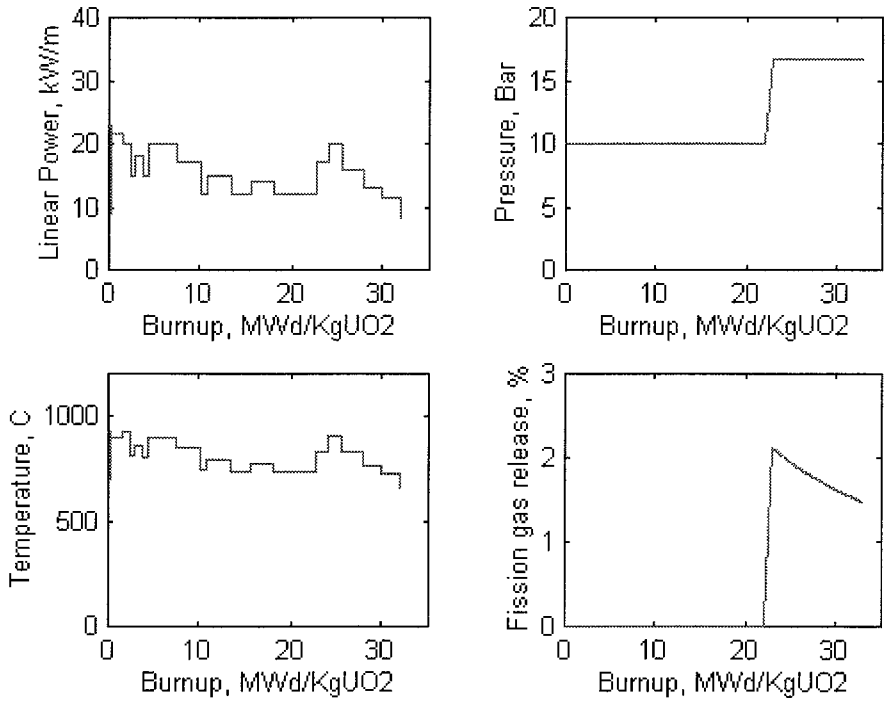

FIG.1. Simplified power history and calculation results corresponding to FUMEX 1.

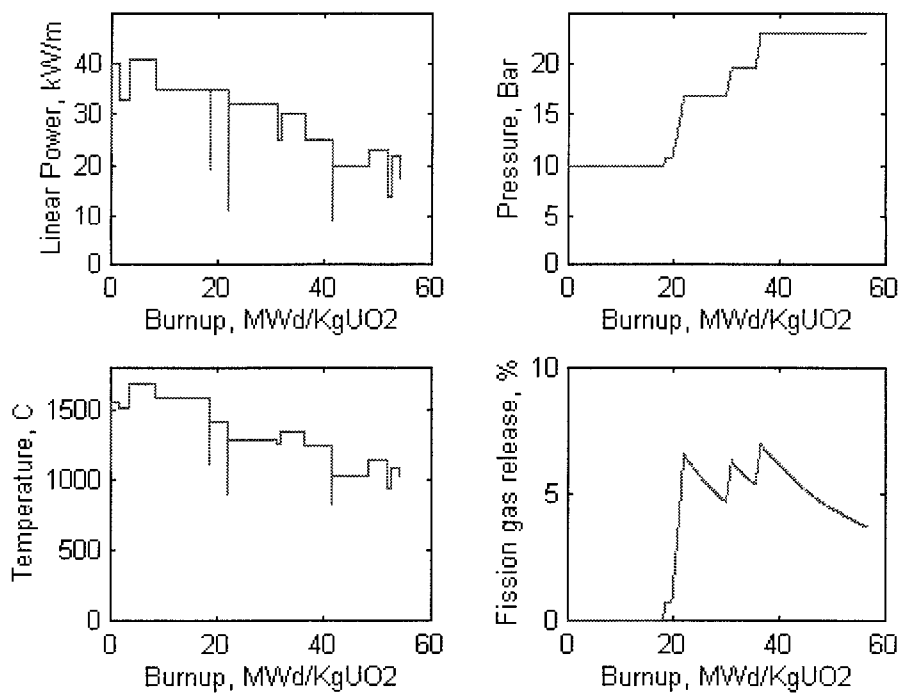

FIG.2. Simplified power history and calculation results corresponding to FUMEX 2.

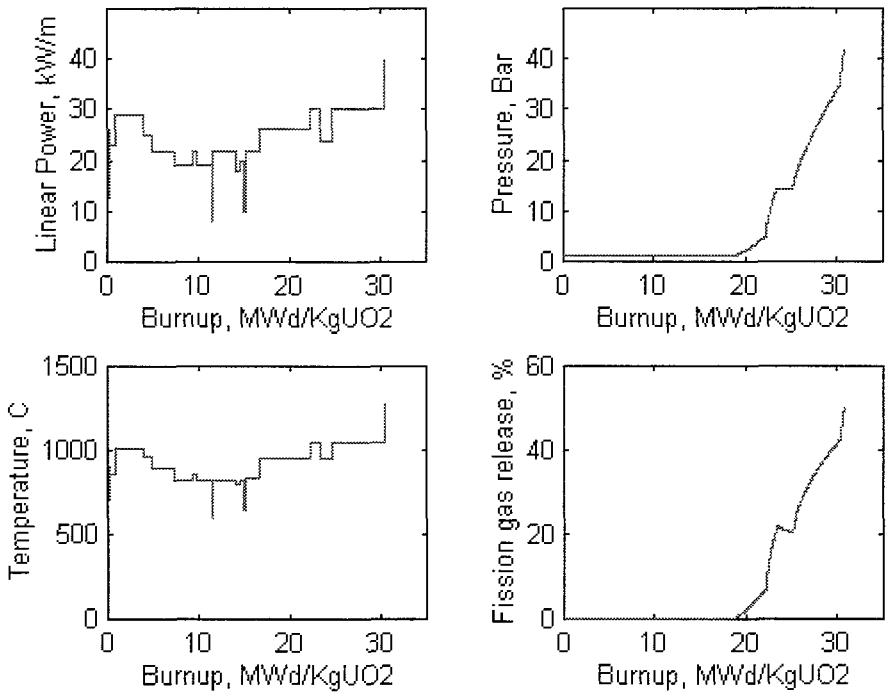

FIG.3. Simplified power history and calculation results corresponding to FUMEX 3 rod 2

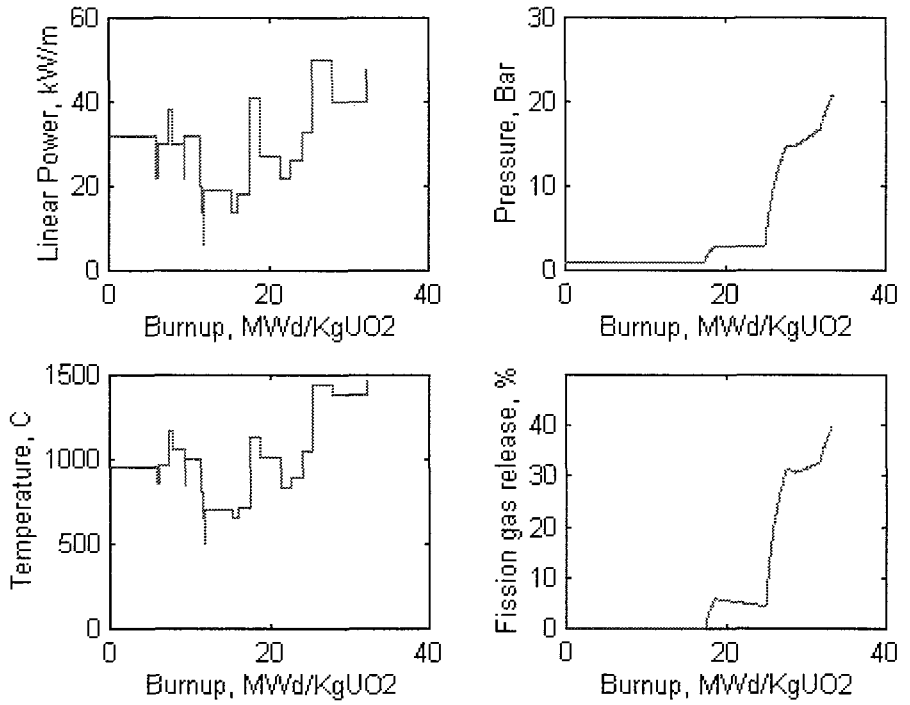

FIG.4. Simplified power history and calculation results corresponding to FUMEX 4 rod B.

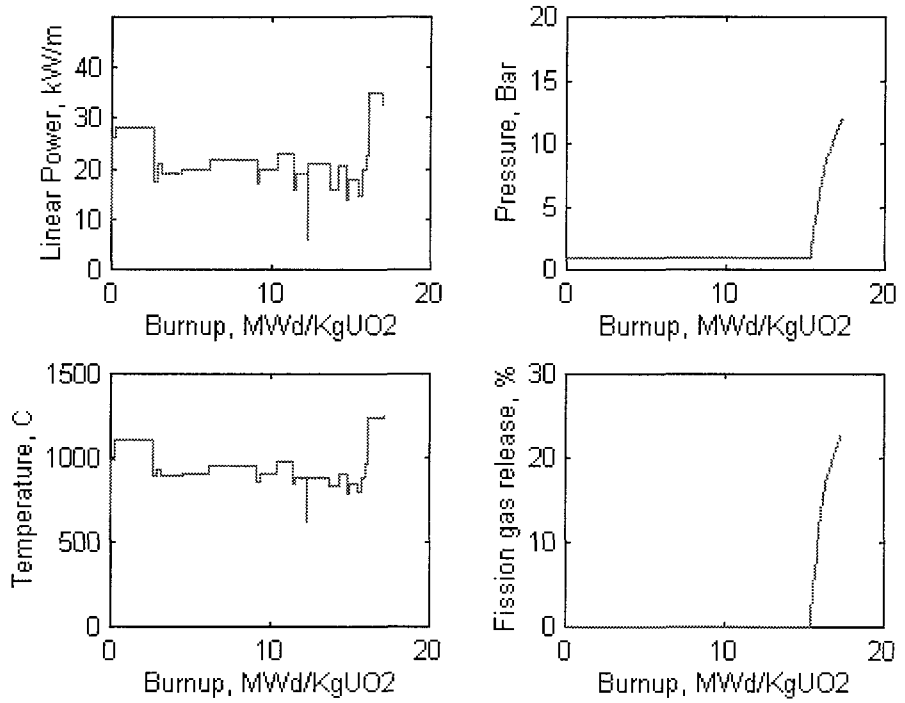

FIG.5. Simplified power history and calculation results corresponding to FUMEX 5.

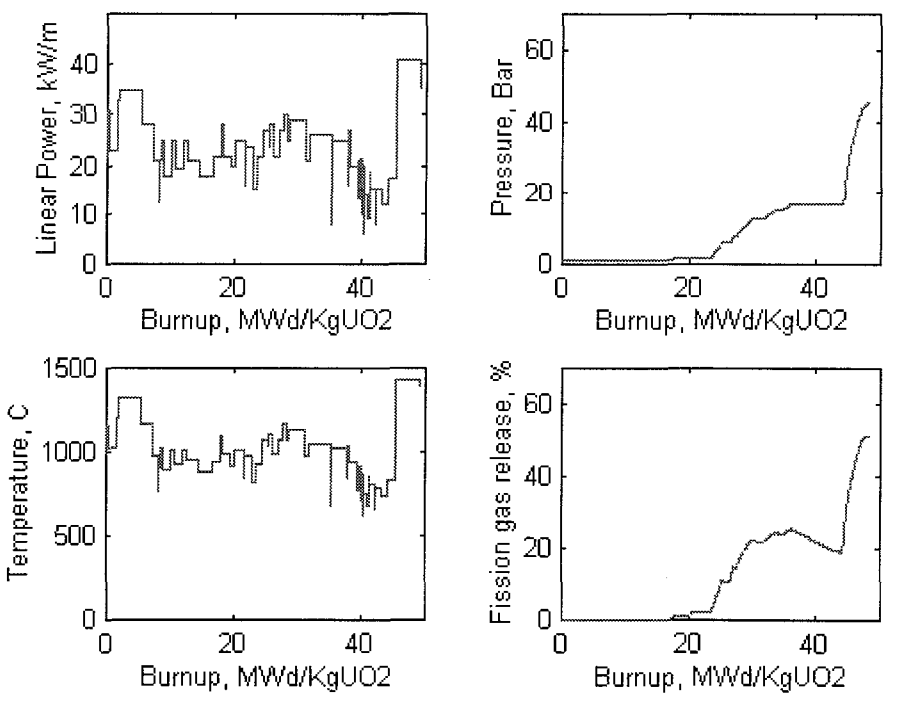

FIG.6. Simplified power history and calculation results corresponding to FUMEX 6F.

TABLE II. COMPARISON BETWEEN DATA OF THE FUMEX EXPERIMENT AND THE PRESENT CALCULATIONS

		experimental	other codes	this code
FUMEX 1	central temperature at 20MWd/kgUO2, °C	740	508–800	734
	FGR at EOL, %	1.8	0.05–2.18	1.47
FUMEX 2	central temp. at 5MWd/kgUO2 and 40kW/m, °C		1210–1820	1584
	FGR at EOL, %	3	1.2–28.8	3.69
	internal rod pressure at power and EOL, bar	20.3	20.1–50	22.9
FUMEX 3 rod 2	central temp. before power ramp, °C	1040	865–1365	1042
	FGR before power ramp, %		0.6–44	42.3
	FGR after power ramp, %		5.3–50.5	50.4
FUMEX 4 rod A	central temp. at start–up and 30 kW/m, °C	1020	876–1398	1067
	central temp. during power ramp, °C	1125	792–1533	1161
	central temp. at EOL, °C	1225	1035–2246	1610
	FRG before power ramp, %		0.3–10.6	7
	FGR during power ramp, %		0.7–26.1	7.1
	FGR at EOL, %		15.4–53.8	38.6
FUMEX 4 rod B	central temp. at start–up, °C	1065	953–1522	957
	central temp. at the top of the ramp, °C	1260	1200–1593	1445
	central temp. at EOL, °C	1290	1213–2203	1482
	FGR at EOL, %		27.5–50	40.3
	pressure at hot standby after power ramp, bar	23.9	3–45.3	19.9
FUMEX 5	FGR before period of high power, %	0	0–43.1	0
	FGR at EOL, %	5.8	1–21.7	2.3
	pressure at start–up, bar	2.3	2.7–66.6	1
	pressure at EOL, bar	9.4	3.9–82.6	12.1
FUMEX 6	FGR at end of base irradiation, %	16.4	7–20.2	19.1
	pressure at end of base irradiation, bar		7.6–79.5	15.7
FUMEX 6F	FGR at EOL, %	45	8.9–38.2	51.2
	pressure at EOL, bar	84.6	40.4–102	44.9
FUMEX 6S	FGR at EOL, %	50	14–50.4	80.6
	pressure at EOL, bar	92.3	40.4–106.7	69.1

5. CONCLUSIONS

Although the results shown above are quite acceptable, the code requires further improvement. For instance, a gas mixing model needs to be included. The code doesn't contain an adequate treatment of the power ramps, which are averaged. The description in the axial direction has to be modified in order to simulate rod elongation. It is expected that these modifications will improve the performance of the code.

ACKNOWLEDGEMENTS

The authors wish to acknowledge Ing. L. Álvarez and Lic. A. Marino for the provision of the data with which the calculations were performed.

REFERENCES

[1] MATHEWS, J.R., The quantitative description of deformation and stress in cylindrical fast reactor fuel pins, in Advances in Nuclear Science and Technology, Vol.6 (1972), Academic Press.

[2] CAILLOT, L., LINET, B., LEMAIGNAN, C., Pellet clad interaction in PWR fuel. Analytical irradiation experiment and finite element modelling, (Proc. SMIRT 12, Stuttgart, Germany, 1993)

[3] DELETE, G., CHARLES, M., "Thermal conductivity of fully dense unirradiated UO_2: a new formulation from experimental results between 100°C and 2500°C and associated fundamental properties", Water Reactor Fuel Element Modelling at High Burnup and its Experimental Support, IAEA–TECDOC–957, IAEA (1997) 203–216.

[4] TIMOSHENKO, S., Theory of elasticity, McGraw Hill, 1951.

[5] PENNY, MARRIOT, Design for creep, McGraw Hill, 1971.

[6] HARRIAGUE, S., COROLI, G., SAVINO, E., BACO, a computer code for simulating a reactor fuel rod performance, Nucl. Eng. and Design 56 (1980) 91–103.

[7] SEGERLIND, L.J., Applied finite element analysis, 2nd Ed., Wiley (1984).

[8] Handbook of materials properties for use in the analysis of light water reactor fuel behavior, MATPRO version 11, NUREG/CR-0497, TREE–1280 (1979).

[9] DENIS, A., PIOTRKOWSKI, R., Simulation of isothermal fission gas release, J. of Nucl. Mater. 229 (1996) 149–154.

[10] DENIS, A., PIOTRKOWSKI, R., A fission gas release model, Water Reactor Fuel Element Modeling at High Burnup and Experimental Support, IAEA-TECDOC-957, IAEA (1997) 455–465.

[11] TURNBULL, J.A., WHITE, R., WISE, C., The diffusion coefficient of Fission Gas Atoms in UO_2, IAEA TC 659/3.5 (1987) 174–181.

[12] WHITE, R., TUCKER, M., A new fission gas release model, J. of Nucl. Mater. 118 (1983) 1–38.

[13] ITO, K.,IWASAKI, R:,IWANO, Y., Finite element model for analysis of fission gas release from UO_2 fuel, J. of Nucl. Sci. and Technol. 22 (2) (1985) 129–138.

[14] NAKAJIMA, T., A comparison between fission gas release data and FEMAXI–IV code calculations, Nucl. Eng. And Design 101 (1987) 267–279.

[15] STAUFFER, D., Introduction to percolation theory, Taylor & Francis, London ans Philadelphia, 1985.

[16] MALDOVÁN, M., DENIS, A., PIOTRKOWSKI, R., Simulation of isothermal fission gas release. An analytical solution, Nucl. Eng. and Design 187 (1999) 327–337.

[17] OLANDER, D., Fundamental aspects of nuclear reactor fuel elements, Technical Information Center, USDOE, 1976.

[18] FRANKLIN, D., ROBERTS, J., LI, C., Low temperature swelling and densification properties of LWR fuels, J. of Nucl. Mater. 125 (1984) 96–103.

[19] MARINO, A., SAVINO, E., HARRIAGUE, S., BACO code version 2.20: a thermomechanical description of a nuclear fuel rod, J.Nucl. Mater. 229 (1996) 155–168.

[20] INTERNATIONAL ATOMIC ENERGY AGENCY, Fuel Modeling at extended burnup, IAEA–TECDOC–998.